

Finite Element Simulation for Predicting the Magnetic Flux Density for Electromagnetic Vibration Energy Harvester [†]

Tunde Toluwalaju ¹, Chung Ket Thein ^{1,*} and Dunant Halim ²

¹ School of Aerospace, University of Nottingham Ningbo China, Ningbo 315104, China; tunde.toluwalaju@nottingham.edu.cn

² Department of Mechanical, Materials and Manufacturing Engineering, University of Nottingham Ningbo China, Ningbo 315104, China; dunant.halim@nottingham.edu.cn

* Correspondence: chungket.thein@nottingham.edu.cn

[†] Presented at 8th International Electronic Conference on Sensors and Applications, 1–15 November 2022; Available online: <https://ecsa-9.sciforum.net>.

Abstract: The current revolution in the field of electromagnetic vibration energy harvester requires that both wireless sensor nodes and relevant power sources are cost and size optimized. While ensuring that during design/fabrication of the sensor's power sources the power deliverable to the sensors is maximum. Flux density dependency on the nature of the magnetic coupling material of VEH magnet-coil transducer is well reported while reports on size optimized but improved performance in the VEH is available. This paper presented on realizing an approach to ensure an accurate prediction of size optimized but maximum power output on the electromagnetic transducer of a VEH. The approach adopted justifiably verify the geometrically determined flux density on a Finite Element Magnetic Method Software (FEMM) on the permanent magnet (NdFeB N52) as a bases for optimization. An empirical formula that predicts size optimized flux density that could be used to predict performance of a miniature energy harvester for wireless sensor nodes application were formulated. For the geometry presented in this work, where, l_c and N_{c-2} are the effective length and turns on the reference coil, the magnetic flux density, coupling coefficients, coil width and transducer thickness was predicted to optimize at 0.4373 T, $0.3978\mu_3 l_c N_{c-2}$ Tmm, 4.00 mm, and 18.40 mm respectively, all corresponding to instances when the flux density per unit volume on the coil was approximately $0.4373/(\mu_3 \bar{v}_{c-2})\text{Tmm}^{-3}$. The above optimized values were measured on magnet-coil geometry with the smallest overall thickness. However, in comparison to other models, the coil thickness in the optimized geometry was not the least.

Keywords: finite element method; magnetic flux density; vibration energy harvester; empirical formula

Citation: Toluwalaju, T.; Thein, C.K.; Halim, D. Finite Element Simulation for Predicting the Magnetic Flux Density for Electromagnetic Vibration Energy Harvester. *Eng. Proc.* **2022**, *4*, x. <https://doi.org/10.3390/xxxxx>

Academic Editor: Francisco Falcone

Published: 1 November 2022

Publisher's Note: MDPI stays neutral with regard to jurisdictional claims in published maps and institutional affiliations.



Copyright: © 2022 by the authors. Submitted for possible open access publication under the terms and conditions of the Creative Commons Attribution (CC BY) license (<https://creativecommons.org/licenses/by/4.0/>).

1. Introduction

A VEH has proven worthy of having the capacity to sustainably supply electrical power to wireless sensor nodes (WSN's) and body sensor networks (bodyNET) [1] by scavenging ambient vibrational energy and converting them into useful electrical energy. The scope of scavenging environmental energy has in the recent attracted the interest because it opens pathway to realizing the sustainable development goals of cutting down carbon footprints which are mostly produces as waste product during energy generation. Previous work concluded structural and electrical based optimization of energy harvester [2]. An innovative approach on the two-degree of freedom (2DOF) linear vibration energy harvester for train application and optimization were analyzed on Multiphysics using result from numerical magnetic field simulation [3]. The model prototype was fabricated and found consistent with the theoretical results obtained. A study on dynamic responses in 2DOF system was based on different electrical coil connection and geometry to

ascertain which connection mode gives an optimum performance concluded that series connection is the best in term of harvested voltage/power, operational bandwidth, and the normalized power [4]. A path to achieving power maximization on a size optimized/miniature AA-battery sized VEH design was reported [5], the author coupled a non-magnetic (tungsten) inertial mass alongside with the axially oriented oscillating magnet to compensate for resonant due to miniaturization. [6,7], reported a ring-shaped coil-magnet transducer architecture of VEH with Halbach configuration where a linear Halbach array concentrates its magnetic field in the inner space of the mechanism where a vertically centered single coil was located to increase the resonant mass within a fixed dimension of the transducer. In a separate attempt, the level of the flux density in the power line were measured using an FEMM software during fabrication indoor power line based magnetic field energy harvester [8]. In a similar endeavor, measuring the flux density using FEMM on an Halbach array was mentioned in [7].

Without a loss of generality, this paper focuses on realizing an approach to ensure an accurate prediction of the optimum overall size that will maximize the coupling coefficient power output on the electromagnetic transducer of a VEH.

2. Harvesters Governing Equation

A vibration energy harvester is a device that scavenge and transform ambient vibration into useable electrical energy that could power sensor nodes. The VEH comprises of a coil placed in the field of a permanent magnet such that during vibration, the coil that is fixed to free end of a fixed-free mechanical structure will freely oscillate. As much as engineers have keen interest to realize the above objectives, cost, and size optimization, remains a valuable pearl held in high esteem during fabrication/design. This work presents a finite element simulation approach to realize size optimization based on the level of the magnetic flux density/coupling in the iron-magnet-coil part of an electromagnetic vibration energy harvester. The focus in this work will be to optimize the iron magnet-coil geometry with the view to realize more compact, lightweight, and cost-effective design iron-magnet-coil designs. Figure 1. shows the general geometry employed to fully characterize the transduction iron-magnet-coil that will be modelled in the FEMM software.

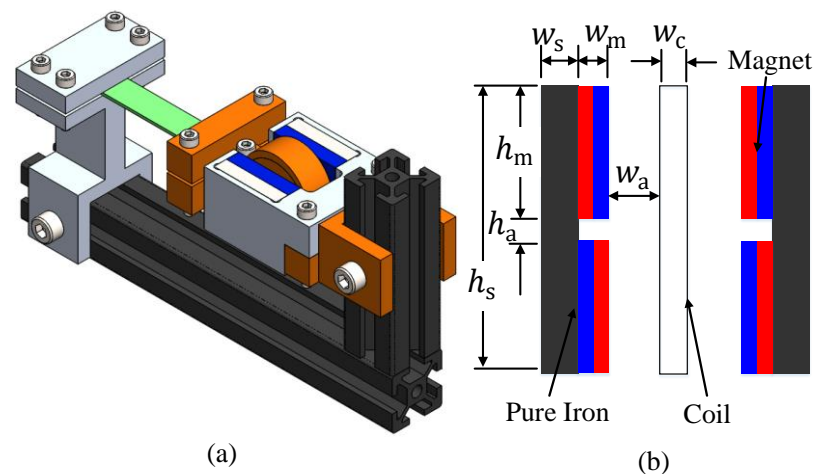


Figure 1. (a) SDOF cantilevered electromagnetic vibration energy harvester and (b) model geometry for the iron-magnet-coil part.

From Figure 1, h_s , h_a , and h_m are the respective heights of pure iron plate which prevent flux leakages, separation distance between coil and magnets, and outer magnet. While w_c , w_s , w_a , and w_m are the respective widths/thickness of the materials earlier mentioned. Equation (1) gives an expression for computing the terms h_c and h_s .

$$h_c = h_s = 2h_m + h_a \tag{1}$$

The sufficient clearance between the coil the magnet, w_a , was fixed to 1.5 mm to prevent contact during excitation. The total width of the iron-magnet-coil was obtained from Figure 1 is shown in Equation (2).

$$w_T = 2(w_s + w_m + w_a) + w_c \quad (2)$$

When the geometry is visualized on a 3D plane, the model protrudes by a fixed length L into the page. During excitation, the magnetic flux of the permanent magnet couples into the freely oscillating coil, hence, voltages are induced in the coil according to the principle of electromagnetic induction. K is defined as the degree of coupling was obtained [9].

$$K = NBl_c c_f \quad (3)$$

where N, B, l_c and c_f are effective turn, flux density, effective length, and coil fill factor. If none of the magnetic flux couples into the coil, an approximately zero voltage is induced in the coil. Therefore, the coil materials are carefully selected (copper in this case) to ensure that highest possible degree of coupling is realized. The selected copper wire material is wound into N turns on a nonconductive circular brace to achieve a total coil width/thickness w_c .

The Maxwell theory reported that divergence and the curl of the flux density where J, H are the current and magnetic field density, μ is permeability of the magnetic material.

$$\nabla \cdot (\mu H) = 0 \quad (4)$$

$$\nabla \times (\mu H) = \mu_0 J \quad (5)$$

The physical meaning of Equations (4) and (5) asserts that for any magnetic system/magnet there are no isolated magnetic poles and circulating magnetic fields are produced by changing electric currents. In the eventuality of using more than one magnet, Equation (4) sets an order for which the transduction magnet must be aligned to allow for continuous flux linkage between the several magnets in such a manner that no pole is isolated while also giving a prediction of a non-changing flux value since external source of electric charge in the system is zero.

3. Iron-Magnet-Coil Simulation and Coupling Equations.

Before the flux density were simulated on FEMM, an initial approach to characterize the flux on a $5 \text{ mm} \times 10 \text{ mm} \times 25 \text{ mm}$ magnet using a Gauss meter actualized to a value of 0.3322 T. However, the FEMM software predicted an average magnet flux density of 0.3421 T which is also measured on the surface center in the Figure 2a and the flux density across the red line are shown in Figure 2b. This measured value diverges from empirical value to about 4.73 %, however, the level of divergence is considered sufficiently accurate while Figure 2b shows that higher flux occurs at the edges of the magnets.

During FEMM simulation of the coil-magnet model, a total of eight (8) magnets of $15 \text{ mm} \times 15 \text{ mm} \times 1 \text{ mm}$ and paired into four (4) groups as shown in Figure 1 and according to Equation (2). FEMM however, predicted average magnetic flux density of 0.04993 T and 0.1007 T at the center of the single and paired magnets respectively as shown in Figure 2b while Figure 2a shows the FEMM pattern on the paired magnet.

Adequate flux/coupling prediction requires insight about the distribution of the flux fields in the coils (i.e., flux density per unit volume (β)). The predicted B values were found consistent with the magnets dimension realizing a β value of $2.74 \times 10^{-4} \text{ Tmm}^{-3}$, $2.234 \times 10^{-4} \text{ Tmm}^{-3}$, and $2.219 \times 10^{-4} \text{ Tmm}^{-3}$ on the $25 \text{ mm} \times 10 \text{ mm} \times 5 \text{ mm}$, $15 \text{ mm} \times 15 \text{ mm} \times 1 \text{ mm}$ paired and $15 \text{ mm} \times 15 \text{ mm} \times 1 \text{ mm}$ single magnet configurations, respectively. From the above, the magnetic flux density on any NdFeB N52 permanent magnet of known volume (v) was obtained as

$$B = \beta v \quad (6)$$

where β is the magnetic flux density per unit volume. It was obtained as the ratio of the magnetic flux density associated with each magnet geometry on the FEMM to its volume.

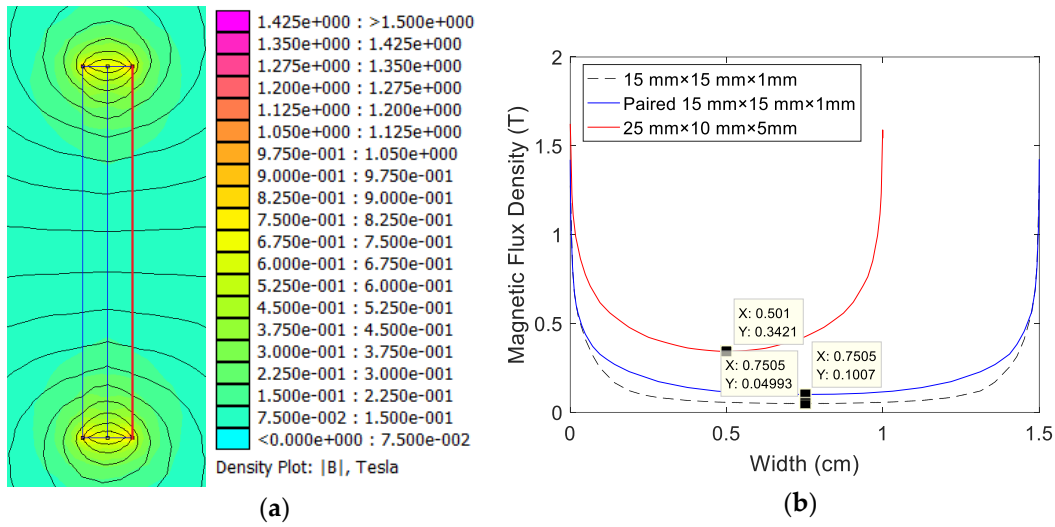


Figure 2. (a) Flux density pattern from FEMM of 15 mm × 15 mm × 1 mm (paired) and (b) flux density line plot for different magnet models.

Considering the transducer geometry, the need to be normalize v and β associated with a single magnet to \bar{v} and $\bar{\beta}$ to account for the coil area where the magnetic flux density was measured in the FEMM arose. Hence, the normalized equation for predicting magnetic flux density in any coil geometry with volume \bar{v} was obtained as

$$B = \bar{\beta} \bar{v} = \bar{\beta} w_c h_s L \quad (7)$$

Using Equation (7), we re-formulate Equation (3) to an equation as shown in Equation (8).

$$K = \bar{\beta} \vartheta N \bar{v} \quad (8)$$

where, ϑ was obtained as the product of the fill factor (c_f), and effective length (l_c). Figure 3b shows a plot of variation of the flux measured on different coil geometry with thicknesses of different components of the model. From Figure 3c, a line of fit and fit equation between B and the coil thickness measured in millimeters (w_c) shown in Equation (8).

$$B = -0.166 \ln w_c + 0.6357 \quad (9)$$

From Equations (3), (8) and (9) an empirical relation between the magnet flux density per unit volume of the transduction coil was obtained as

$$\bar{\beta} = (1/\bar{v})(-0.166 \ln w_c + 0.6357) \quad (10)$$

Equations (8) and (10) are sufficient to make a prediction of the flux density per volume of a coil and the coupling coefficient on any coil geometry, respectively.

Using the $w_c = 2$ mm as reference configuration, while keeping effective length (l_c) and packing density factor (c_f) approximately equal over different width size implies that to ensure that h_s remains as shown in Equation (1), the term N and \bar{v} will approximately change with each configuration according to Equation (11).

$$N_{c-i} = \mu_i N_{c-2}, \quad i = 1, 2, \dots, n \quad (11)$$

where $\mu_i = (w_{c-i}/w_{c-2})$, N_{c-i} and w_{c-i} are the ratio of the coil width, the total coil turn and width of the i^{th} coil while N_{c-2} , and w_{c-2} the total coil turns and width of the

reference coil. An Equation like Equation (11) in term of the volume ratio $\bar{v}_{c-i} = \mu_i \bar{v}_{c-2}$ also exists.

4. Results

As earlier mentioned, w_m and w_a are fixed thicknesses of the magnet and air space separating the coil and the magnet respectively. During FEMM simulation of the iron-magnet-coil part of the harvester, these two parameters are fixed while w_s and w_c were varied to realized different models of the coils while ensuring that the variable l_c and c_f are equal across different realized coil configurations and that w_s was carefully chosen to ensure that an approximately zero flux leakage occurs on the iron.

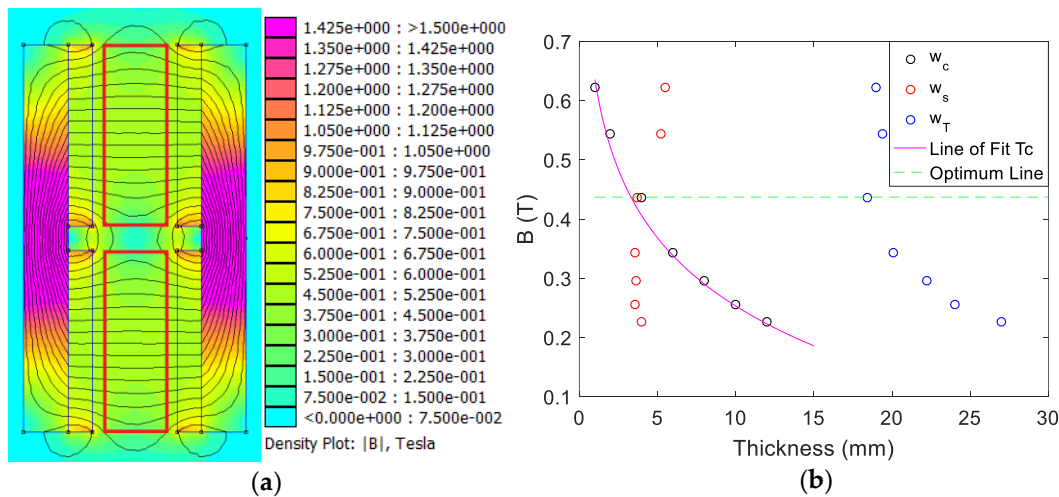


Figure 3. (a) Magnet-coil simulation output on FEMM for 4 mm coil width, and (b) variation of B with geometry thicknesses.

Figure 3a shows the result and legends from the FEMM simulation respectively. The location of the coil corresponding to each simulation is outlined in thick red lines. Table 1 shows a summary of the flux density B and leakage sufficient iron cladding thickness over different coil width (w_c). Different coil width w_c reported in Table 1 was achieved by winding the copper wire having a total effective length l_c into a coil loop of total turns N while ensuring equal l_c and $c_f = 90.97\%$ [10] for all geometries.

Table 1. Summary of the flux density (B) and leakage proof iron cladding thickness (w_s) coil thickness (w_c), and total model thickness (w_T) for different design geometries.

Model	w_c (mm)	w_s (mm)	w_T (mm)	N_{c-2}	B (T)	$\bar{\beta}(Tmm^{-3})$	K (Tmm)
1	1.00	5.50	19.00	$\mu_1 N_{c-2}$	0.6226	$0.6226/(\mu_1 \bar{v}_{c-2})$	$0.5663 \mu_1 l_c N_{c-2}$
2	2.00	5.20	19.40	$\mu_2 N_{c-2}$	0.5450	$0.5450/(\mu_2 \bar{v}_{c-2})$	$0.4957 \mu_2 l_c N_{c-2}$
3	4.00	3.70	18.40	$\mu_3 N_{c-2}$	0.4373	$0.4373/(\mu_3 \bar{v}_{c-2})$	$0.3978 \mu_3 l_c N_{c-2}$
4	6.00	3.53	20.06	$\mu_4 N_{c-2}$	0.3438	$0.3438/(\mu_4 \bar{v}_{c-2})$	$0.3127 \mu_4 l_c N_{c-2}$
5	8.00	3.60	22.20	$\mu_5 N_{c-2}$	0.2955	$0.2955/(\mu_5 \bar{v}_{c-2})$	$0.2688 \mu_5 l_c N_{c-2}$
6	10.00	3.56	24.00	$\mu_6 N_{c-2}$	0.2562	$0.2562/(\mu_6 \bar{v}_{c-2})$	$0.2331 \mu_6 l_c N_{c-2}$
7	12.00	4.00	27.00	$\mu_7 N_{c-2}$	0.2267	$0.2267/(\mu_7 \bar{v}_{c-2})$	$0.2062 \mu_7 l_c N_{c-2}$

The dotted green line in Figure 3b shows the level of flux at which the harvesters become size (thickness) optimized in term of the flux density (B) and degree of coupling (K). This is because the overall width of the magnet-coil is the minimum which corresponding to the 4 mm coil thickness. Based on this estimation, the optimized flux, coupling coefficient, coil thickness and overall transducer thickness for the model herein described was predicted at a value of 0.4373 T, $0.3978 \mu_3 l_c N_{c-2}$ Tmm, 4.00 mm and 18.4 mm respectively corresponding to the intersection of the flux density on the iron cladding and

the transduction coil. This optimum point corresponds to $\bar{\beta} = 0.4373/(\mu_3 \bar{v}_{c-2}) Tmm^{-3}$. Since, μ_i is linearly dependent on w_{c-i} , and μ_i is an inverse and direct relationship the last two columns of Table 1 respectively, therefore an inverse relation will exist between K and $\bar{\beta}$ contrary to expectation since it is very basic to think that the flux and harvested power will become size optimized on highest possible coupling. However, this is not the case because higher coupling will always produce an undesirable larger damping, hence a reduced harvested power [9].

During design, it is advised to concentrate the transducer mass in the non-magnetic coil brace to ensure accuracy of flux prediction while targeting expected resonance.

5. Conclusions

From the forgone discussions and analysis, the following conclusions were reached

1. Since the flux is measured in the region where the coil is positioned, it is recommended that the inertial mass of the transducer should be concentrated in the coil to allow for resonant variation with little divergence from predicted values.
2. A nonlinear relationship existed between K and β . Both were respectively optimized at $0.3978\mu_3 l_c N_{c-2} Tmm$ and $0.4373/(\mu_3 \bar{v}_{c-2}) Tmm^{-3}$.
3. For any two coils, the coupling coefficient is not only a function of the flux density, but also a function of the ratio of the width of the second coil to the reference coil.
4. Given any coil of known volume, it is possible to make a relatively accurate prediction of the magnetic flux density using Equation (10) when such coil is placed in the field of permanent magnet that are paired and arranged as shown in Figure 1.
5. The above prediction and approaches shall be verified in future experimental approach which shall be used to test performances of prototypes.

Author Contributions:

Funding:

Institutional Review Board Statement:

Informed Consent Statement:

Data Availability Statement:

Conflicts of Interest:

References

1. He, T.; Guo, X.; Lee, C. Flourishing energy harvesters for future body sensor network : from single to multiple energy sources. *ISCIENCE* **2021**, *24*, 101934, .
2. Foong, F.M.; Thein, C.K.; Yurchenko, D. A two-stage electromagnetic coupling and structural optimisation for vibration energy harvesters. *Smart Mater. Struct.* **2020**, *29*, 85030.
3. Perez, M.; Chesné, S.; Jean-mistral, C.; Billon, K.; Augez, R.; Clerc, C. A two degree-of-freedom linear vibration energy harvester for tram applications Output . *Mech. Syst. Signal Process.* **2020**, *140*, 106657, .
4. Toluwalaju, T.I.; Thein, C.; Halim, D.; Yang, J. Dynamic responses of the 2DOF electromagnetic vibration energy harvester through different electrical coil connections. *Mech. Syst. Signal Process.* **2023**, *184*, 109709.
5. Yasar, O.; Ulsan, H.; Zorlu, O.; Sardan-Sukas, O.; Kulah, H. Optimization of AA-Battery Sized Electromagnetic Energy Harvesters: Reducing the Resonance Frequency Using a Non-Magnetic Inertial Mass. *IEEE Sens. J.* **2018**, *18*, 4509–4516.
6. Arcos, R.; Romeu, J.; Ordo, V. A high-performance electromagnetic vibration energy harvester based on ring magnets with Halbach configuration. *Energy Convers. Manag. X* **2022**, *16*, 100280.
7. Salauddin, M.; Halim, M.A.; Park, J.Y. A magnetic-spring-based, low-frequency-vibration energy harvester comprising a dual Halbach array. *Smart Mater. Struct.* **2016**, *25*, 95017.
8. Maharjan, P.; Cho, H.; Park, J.Y. An indoor power line based magnetic field energy harvester for self-powered wireless sensors in smart home applications. *Appl. Energy* **2018**, *232*, 398–408.
9. Toluwalaju, T.I.; Thein, C.K.; Halim, D. An Effect of Coupling Factor on the Power Output for Electromagnetic Vibration Energy Harvester. *Eng. Proc.* **2021**, *10*, 5.

10. Toluwalaju, T.I.; Thein, C.; Halim, D. A novel redefined electromagnetic damping equation for vibration energy harvester. In Proceedings of the International Conference on Electrical, Computer, Communications and Mechatronics Engineering, ICECCME 2021, Mauritius, Mauritius, 7–8 October 2021; pp. 7–8.